Fundamental equation of state for ethylene oxide based on a hybrid dataset

Monika Thol[a], Gábor Rutkai[b], Andreas Köster[b], Mirco Kortmann[a], Roland Span[a], Jadran Vrabec[b,*]

[a]*Lehrstuhl für Thermodynamik, Ruhr-Universität Bochum, Universität Str. 100, 44801 Bochum, Germany*
[b]*Lehrstuhl für Thermodynamik und Energietechnik, Universität Paderborn, Warburger Str. 100, 33098 Paderborn, Germany*

Abstract

An empirical fundamental equation of state correlation is presented for ethylene oxide. The correlation is explicit in terms of the Helmholtz energy and it can be used to calculate all thermodynamic properties. The underlying dataset consists of experimental and molecular simulation data. The experimental data cover almost exclusively the gaseous phase and are available for temperatures from the triple point up to the critical point. Molecular simulation data are used to extend the validity to the liquid state and up to a maximum temperature of 1000 K and a maximum pressure of 700 MPa.

Keywords: thermodynamic properties, fundamental equation of state, molecular simulation, ethylene oxide

1. Introduction

A sufficient amount of reliable thermodynamic data is essential for the design and optimization of almost any process in the chemical industry. Currently, databases alone cannot meet the increasing requirements of process engineering. Mapping the entire thermodynamic property spectrum of a given fluid is often impossible using laboratory experiments due to the associated financial cost, time investment, and potentially extreme measuring conditions. Empirical equations of state (EOS) correlations are one solution for this problem, because they rationalize and summarize experimental data, offering a built-in interpolation and extrapolation scheme for general engineering purposes. Empirical correlations that represent the fundamental equation of state (FEOS) are particularly beneficial [1]. A FEOS can be expressed in terms of various thermodynamic potentials. However, independent on which representation is chosen, it contains the complete property information about the system: Once a thermodynamic potential is explicitly given as a function of its natural variables, every other thermodynamic property is simply a combination of its derivatives with respect to its natural variables.
The construction of a FEOS that covers the entire fluid region of industrial relevance typically faces the problem of scarce experimental input data. Molecular modelling and simulation have evolved to a point of acceptance in the applied sciences and are a potential solution to satisfy the need for thermodynamic data. Molecular simulation yields macroscopic properties exclusively from microscopic information. Accordingly, its predictive capabilities are, in principle, only limited by the quality of the molecular interaction model that represents the investigated substance. While molecular simulation techniques (Monte Carlo and molecular dynamics) have a huge advantage over experimental measurements when it comes to speed and cost efficiency, the number of molecular interaction models that can really offer an alternative to laboratory measurements, not just on the qualitative, but also on the quantitative level, increased significantly only over the last decade [2]. Extreme temperatures or pressures are not limiting factors for molecular simulation, and any thermodynamic property is obtainable from such calculations, including the derivatives of the chosen thermodynamic potential of the FEOS.
Ethylene oxide is the 14th most produced organic chemical and its global production rate is expected to exceed 27 million tons per year by 2017. Due to its chemical reactivity, it is a vital chemical compound used as an intermediate to produce a wide range of consumer products and other non-consumer chemicals. Its reactive nature also makes the substance itself particularly hazardous: it is carcinogenic, mutagenic, and highly flammable at room temperature. It is not a surprise that the experimental data available in the literature are too few to support FEOS

*Corresponding author: Jadran Vrabec, Warburger Str. 100, 33098 Paderborn, Germany, Tel.: +49-5251/60-2421, Fax: +49-5251/60-3522, Email: jadran.vrabec@upb.de

development. Therefore, the approach of combining the available experimental data with straightforwardly obtainable molecular simulation data is one option for constructing a hybrid dataset as a basis for FEOS correlation [3], which was the target of this work.

2. Fundamental equation of state correlation

The present FEOS correlation is explicit in terms of the Helmholtz energy a, which can be separated into an ideal gas part a^{o} and a residual part a^{r}

$$\alpha(T,\rho) = \frac{a^{\mathrm{o}}(T,\rho) + a^{\mathrm{r}}(T,\rho)}{RT} = \alpha^{\mathrm{o}}(\tau,\delta) + \alpha^{\mathrm{r}}(\tau,\delta), \tag{1}$$

with the inverse reduced temperature $\tau = T_{\mathrm{c}}/T$, the reduced density $\delta = \rho/\rho_{\mathrm{c}}$, and the molar gas constant $R = 8.3144621\,\mathrm{J\cdot mol^{-1}\cdot K^{-1}}$ [4] (for specific calculations the molar mass $M = 44.05256\,\mathrm{g\cdot mol^{-1}}$ should be used). The critical temperature $T_{\mathrm{c}} = 468.92$ K was taken from Ref. [5] and the critical density $\rho_{\mathrm{c}} = 7.32\,\mathrm{mol\cdot dm^{-3}}$ was determined during the present fit. The ideal contribution α^{o} can be calculated from the isobaric heat capacity of the ideal gas state c_p^{o}

$$\frac{c_p^{\mathrm{o}}}{R} = 4 + \sum_{k=3}^{5} v_k \frac{(u_k/T)^2 \exp(u_k/T)}{[\exp(u_k/T) - 1]^2}, \tag{2}$$

where $u_3 = 1330$ K, $u_4 = 2170$ K, $u_5 = 4470$ K, $v_3 = 6.79$, $v_4 = 4.53$, $v_5 = 3.68$. The ideal part of the reduced Helmholtz energy α^{o}, integrated from Eq. (2), is

$$\begin{aligned} \alpha^{\mathrm{o}} &= \ln\delta + 3\ln\tau + a_1 + a_2\tau \\ &+ \sum_{k=3}^{5} v_k \ln\left[1 - \exp(-u_k\tau/T_{\mathrm{c}})\right], \end{aligned} \tag{3}$$

where $a_1 = 7.2881975$, $a_2 = -2.782872$, while u_k and v_k are the same as those in Eq. (2). The integration constants a_1 and a_2 were specified such that the enthalpy $h = 0\ \mathrm{kJ\cdot kg^{-1}}$ and the entropy $s = 0\ \mathrm{kJ\cdot kg^{-1}\cdot K^{-1}}$ at $T_0 = 298.15$ K and $p_0 = 1$ atm, and the corresponding ideal gas density is $\rho_0 = p_0/(RT_0)$. A comparison of Eq. (2) with the available literature data is shown in Fig. 1. The c_p^{o} values used in the fit were published by Chao et al. [6]. The uncertainty of Eq. (2) is ±0.1% for temperatures above $T = 350$ K. For lower temperatures, the deviations increase up to ±0.5%.

The empirical formula that represents the residual part of the reduced Helmholtz energy α^{r} consists of five polynomial, five exponential, and five Gaussian bell-shaped terms

$$\begin{aligned} \alpha^{\mathrm{r}}(\tau,\delta) &= \sum_{k=1}^{5} n_k \tau^{t_k} \delta^{d_k} + \sum_{k=6}^{10} n_k \tau^{t_k} \delta^{d_k} \exp(-\delta^{l_k}) \\ &+ \sum_{k=11}^{15} n_k \tau^{t_k} \delta^{d_k} \exp(-\eta_k(\delta - \epsilon_k)^2 - \lambda_k(\tau - \gamma_k)^2). \end{aligned} \tag{4}$$

Table 1 lists the corresponding parameters. Non-analytic terms [1] for the critical region of ethylene oxide were not considered in this work due to their complexity and the poor experimental data situation.

3. Underlying dataset

3.1. Experimental data

Although ethylene oxide is important for the chemical industry, the corresponding experimental data are very limited. Table 2 summarizes all experimental data that are available in the literature, and Fig. 2 shows the distribution of these data with respect to the homogeneous regions.

For the homogeneous density there is only one comprehensive dataset by Walters & Smith [5]. Additionally,

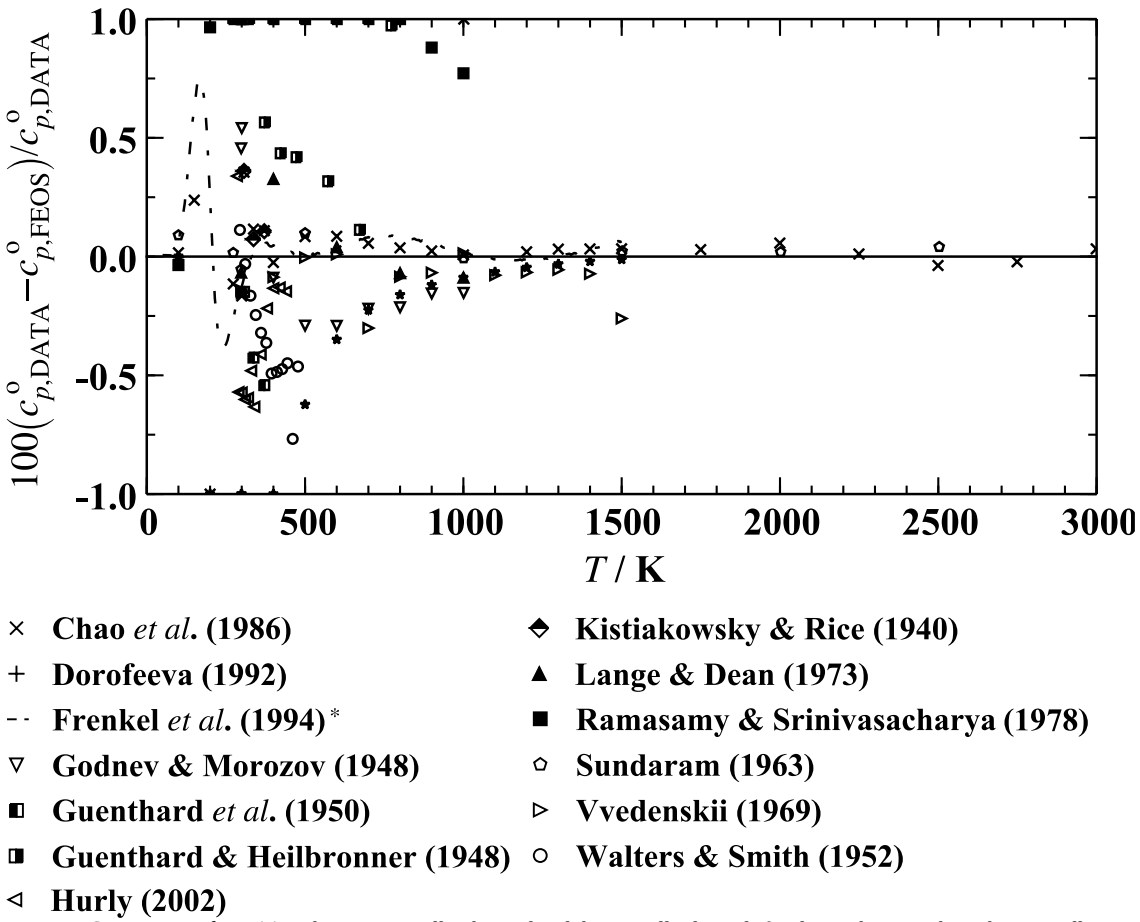

Figure 1: Comparison of Eq. (2) with experimentally obtained and theoretically derived c_p^o values. The asterisk marks an ancillary equation.

Table 1: Parameters for the residual part of the reduced Helmholz energy $\alpha^r(\tau, \delta)$ according to Eq. (4).

k	n_k	t_k	d_k	l_k	η_k	λ_k	γ_k	ϵ_k
1	0.3805675D-01	1.000	4					
2	0.1359482D+01	0.312	1					
3	-0.1833370D+01	0.860	1					
4	-0.5754450D+00	1.114	2					
5	0.1536490D+00	0.500	3					
6	-0.1598130D+01	2.100	1	2				
7	-0.6826090D+00	1.700	3	2				
8	0.6436960D+00	0.754	2	1				
9	-0.5353070D+00	2.500	2	2				
10	-0.1872220D-01	0.900	7	1				
11	0.1238840D+01	2.180	1		1.010	1.12	0.874	0.7202
12	-0.4315460D+00	3.500	1		1.650	2.16	0.617	0.9110
13	-0.2295870D+00	2.340	3		0.896	0.91	0.476	0.6880
14	-0.1931280D+02	4.330	3		22.000	196.00	1.24	0.9100
15	-0.5283590D-01	3.900	2		1.730	0.13	0.562	1.2100

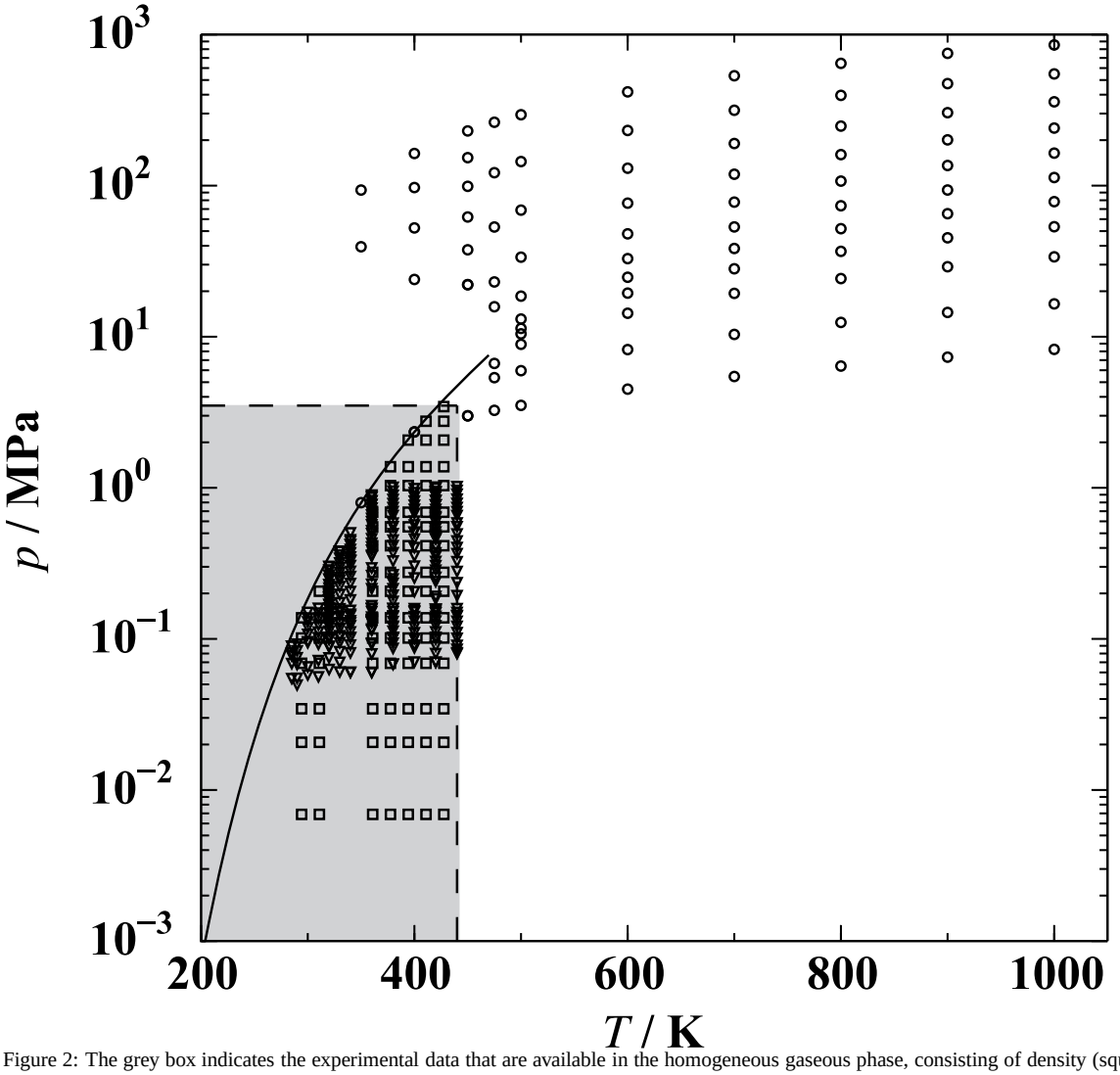

Figure 2: The grey box indicates the experimental data that are available in the homogeneous gaseous phase, consisting of density (squares) and speed of sound (triangles) values. Molecular simulation data were generated in this work, containing six different Helmholtz energy derivatives at each state point (circles).

there is only a single data point located in the liquid region (but not at saturation), which was published by Lide [7]. However, during the data preparation it turned out that this data point is actually located within the two-phase region so that it was not considered in the following. Hence, there are only experimental density data available for the gaseous phase. The situation is almost the same for the speed of sound. The only measurements were made by Hurley [8] for the gaseous phase. All remaining experimental data are associated with the vapor-liquid equilibrium (VLE). For the vapor pressure, 99 data points are available, but most of them were measured at temperatures below 310 K. For the saturated liquid density, only 51 data points were published, and again, most of them were measured in the lower temperature region. For the saturated vapor density as well as for the isobaric heat capacity of the saturated liquid, only one dataset is available. Finally, there are eight data points for the enthalpy of vaporization that are in a narrow temperature range from 283 K to 299 K.

3.2. Molecular simulation data

The experimental data situation for ethylene oxide shows that it is a suitable fluid to apply the approach of fitting a FEOS on the basis of a hybrid dataset as introduced by Rutkai et al. [3]. This method is supported by the statistical mechanical formalism proposed by Lustig [45, 46]. The formalism was designed to yield any derivative of the residual Helmholtz energy $A^{\mathrm{r}}_{xy} = \partial^{x+y}\alpha^{\mathrm{r}}(T,\rho)/\partial(1/T)^x/\partial\rho^y \cdot (1/T)^x\rho^y$ (for $x > 0$ or $y > 0$) from a single molecular simulation run for a given state point, yielding exactly those derivatives that are required

Table 2: Experimental data for ethylene oxide from the literature. The original units were converted into SI units and the temperature is given in terms of the international temperature scale of 1990 standard (ITS-90). Data points calculated from an ancillary equation are marked with an asterisk.

Source	Year	Data points	Temperature range (K)	Pressure range (MPa)
Homogeneous density				
Lide [7] (1)	2005	1	273.15	0.101325
Walters & Smith [5] (1)	1952	81	294–428	0.006–3.448
Overall (3)		*82*	*273–428*	*0.006–3.448*
Vapor pressure				
Calado et al. [9]	1996	1	182.33	0.0001
Chao et al. [6]	1986	1	283.71	0.101325
Coles & Popper [10]	1950	17	273–305	0.067–0.221
Giauque & Gordon [11]	1949	14	223–286	0.004–0.108
Giles & Wilson [12]	2006	2	298–349	0.174–0.767
Gillespie et al. [13]	1985	2	283–299	0.101–0.174
Hess & Tilton [14]	1950	1	293.14	0.1462
Kistiakowsky & Rice [15]	1940	1	283.84	0.101325
Lide [7]	2005	3	283–284	0.101–0.100
Maass & Boomer [16]	1922	21	216–286	0.002–0.110
McDonald et al. [17]	1959	11	284–239	0.103–0.012
Mock & Smith [18]	1950	10	322–423	0.379–3.827
Olson [19]	1977	3	273–324	0.065–0.394
Frenkel et al. [20]*	2013	17	160–469	0.000–7.207
Walters & Smith [5]	1952	12	294–469	0.151–7.192
Overall (3)		*99*	*182–423*	*0.000–3.827*
Saturated liquid density				
Auwers [21]	1918	2	279.20	–
Comelli & Francesconi [22]	1991	11	288–304	–
Comelli & Francesconi [23]	1995	1	298.15	–
Comelli & Francesconi [24]	1996	2	298–314	–
Francesconi & Comelli [25]	1994	1	298.15	–
Francesconi & Comelli [26]	1995	1	298.15	–
Maass & Boomer [16]	1922	16	222–294	–
Olson [19]	1977	3	273–324	–
Perkinsen [27]	1893	1	280.15	–
Frenkel et al. [20]*	2013	17	160–469	–
Walters & Smith [5]	1952	12	294–469	–
Wurtz [28]	1863	1	273.15	–
Overall (3)		*51*	*222–469*	
Saturated vapor density				
Olson [19]	1977	3	273–324	–
Frenkel et al. [20]*	2013	20	377–469	–
Walters & Smith [5]	1952	12	294–469	–
Overall (3)		*15*	*273–469*	
Speed of sound				
Hurly [8]	2002	334	285–440	0.049–1.020
Overall (3)		*334*	*285–440*	*0.049–1.020*
Isobaric heat capacity				
Giauque & Gordon [11]	1949	22	166–284	*vapor pressure*
Overall (3)		*22*	*166–284*	*vapor pressure*
Enthalpy of vaporization				
Cox & Pilcher [29]	1970	1	298.10	–
Rowley et al. [30] * (2)	2006	30	160–423	–
Giauque & Gordon [11]	1949	1	283.65	–
Lange & Dean [31]	1973	1	283.75	–
Lide [7]	2005	2	283–299	–
Matheson [32] *	1980	5	233–294	–
Reid et al. [33]	1977	1	283.66	–
Timmermans [34]	1965	1	288.10	–
Walters & Smith [5] *	1952	11	294–461	–
Washburn [35]	(1926–1933)	1	286.10	–
Yaws [36] *	1977	15	173–454	–
Overall (3)		*8*	*283–299*	
Ideal isobaric heat capacity				
Chao et al. [6]	1986	27	100–2999	–
Dorofeeva [37]	1992	16	100–1501	–
Frenkel et al. [38] *	1994	291	50–1500	–
Godnev & Morozov [39]	1948	9	298–1001	–
Guenthard et al. [40]	1950	3	307–372	–
Guenthard & Heilbronner [41]	1948	8	298–774	–
Hurly [8]	2002	12	285–441	–
Kistiakowsky & Rice [15]	1940	3	307–372	–
Lange & Dean [31]	1973	5	298–1001	–
Ramasamy & Srinivasacharya [42]	1978	12	100–1001	–
Sundaram [43]	1963	8	100–2503	–
Vvedenskii [44]	1969	14	298–1500	–
Walters & Smith [5]	1952	12	294–478	–
Overall (3)		*129*	*100–2999*	

(1) One of the data points is located in the two-phase region and was thus neglected in the following.
(2) Calculated from the Clausius-Clapeyron equation.
(3) The overall values do not include any data derived from ancillary equations.

by the FEOS to calculate any thermodynamic property as a combination of these derivatives. This approach offers a convenient route to obtain an arbitrary number of truly independent thermodynamic properties, and its capability to support FEOS development was recently tested [3]. In the present work, an extensive dataset was generated containing the six derivatives A^{r}_{00}, A^{r}_{10}, A^{r}_{01}, A^{r}_{20}, A^{r}_{11}, and A^{r}_{02} at 92 state points that are well distributed in the homogeneous fluid regions using the molecular simulation tool *ms*2 [47, 48]. The potential accuracy of the results is, of course, limited by the underlying molecular interaction potential model. However, our previous findings showed that molecular models tend to perform well in the homogeneous fluid regions when comparing A^{r}_{xy} simulation results to available FEOS correlations if the molecular model was optimized to experimental VLE data [3].

4. Simulation details

At each state point 500 particles were sufficiently equilibrated and then sampled for 2 million production cycles with *NVT* Monte Carlo simulations [49]. Electrostatic long-range corrections were approximated by the reaction field method [50]. The residual Helmholtz energy was determined by Widom's test particle insertion [51]. The simulations were based on a molecular interaction model by Eckl et al. [52], which won the Fourth Industrial Fluid Properties Simulation Challenge in 2008 [53]. It consists of three Lennard-Jones (LJ) sites and a point dipole located at the geometric center of the molecule. Two sites were used to represent the methylene groups via the united atom approach, the third one represents the oxygen atom. The internal degrees of freedom were neglected due to the relatively small size of the molecule. The corresponding molecular parameters can be found in Ref. [52] and in the appendix. The model was optimized using the correlations by DIPPR [30] for vapor pressure, saturated liquid density, and heat of vaporization.

5. Evaluation of the fundamental equation of state

The accuracy of the FEOS was determined by comparisons of calculated property values to experimental and simulation data. The present statistical comparisons are based on the relative deviation of a given property X, defined as

$$\Delta X = 100 \left(\frac{X_{\mathrm{data}} - X_{\mathrm{FEOS}}}{X_{\mathrm{data}}} \right). \tag{5}$$

With this definition, the average absolute relative deviation is defined as

$$\mathrm{AAD} = \frac{1}{N} \sum_{i=1}^{N} |\Delta X_i| \,, \tag{6}$$

where N is the number of data points. Average absolute relative deviations between experimental data and values calculated from the FEOS are given for different properties in Tables 3 and 4. Table 3 compiles these deviations separately for the vapor phase, the liquid phase, the critical region, and three density ranges of the supercritical region. Saturation properties were also compared with the FEOS, i.e. not with the ancillary equations that are given in Appendix A. The comparisons for vapor pressure and saturated densities were divided into three different ranges of the reduced temperature T/T_{c}, cf. Table 4.

As mentioned above, there are only homogeneous density data available for the gaseous phase. Fig. 3 shows the deviations of the FEOS from the data by Walter & Smith [5]. For temperatures below $T = 360$ K, the deviations were within 0.6%. Higher temperatures were reproduced within 0.1%. Approaching the phase boundary, deviations increase up to 2.5%. As shown in the following, these authors also measured VLE data, which are not consistent with other available data. Thus, the increasing deviations near the phase boundary may be due to a problem within the measurements. Further experimental measurements are needed to verify this assumption.

In Fig. 4, comparisons for the vapor pressure are presented. The first plot shows that most of the data were measured up to $T = 300$ K. For higher temperatures, there are only experimental data by Walter & Smith [5] that were reproduced within 0.8%. One single data point measured by Giles & Wilson [12] in 2006 at $T = 348.15$ K was reproduced within 0.5%. Because it is the only available data point, it can only be treated as a rough guide for the reasonable behavior of the FEOS in that region. Ancillary equations provided by DIPPR [30] and by the Thermo Data Engine (TDE) [20] were also taken into account. Both equations were developed independently,

but they agree within an uncertainty of 2%. Molecular simulation data by Eckl et al. [52] and simulation results from this work are shown for completeness. In the second plot, the vapor pressure deviations are shown with a higher resolution. For 220 K < T < 300 K several datasets are available. Measurements by Giauque & Gordon [11] (AAD_{LT} = 0.16%, AAD_{MT} = 0.07%) were reproduced within 0.1% for T > 235 K. Data at lower temperatures were within 0.6%. Data by Coles & Popper [10] (AAD_{LT} = 1.23%, AAD_{MT} = 0.31%) were represented within 0.3 % for T > 280 K, and those by McDonald et al. [17] (AAD_{LT} = 0.18%) scatter within 0.4%. Below this region (T < 220 K) different trends can be noticed. The ancillary equation from TDE [20] agrees with the present FEOS within 0.7%. The opposite trend can be seen for the ancillary equation by DIPPR [30]. Further measurements are required to definitively determine which source is more correct.

Fig. 5 shows comparisons for the saturated liquid density. Again, two different temperature ranges can be noticed. In the upper temperature range (T > 310 K), only measurements by Walters & Smith [5] are available. Compared to the data by Maass & Boomer [16], an offset of about 1.7% at T = 290 K can be observed. Between 288 K < T < 314 K there are several datasets by Comelli & Francesconi [22, 23, 24, 25, 26] available. These support the trend of the measurements of Walters & Smith [5]. However, fitting these data would lead to an unphysical bend in the phase boundary, and they were thus not included in the present fit. To verify the data by Maass & Boomer [16] (AAD_{LT} = 0.11%, AAD_{MT} = 0.78%) that are within 0.2%, measurements between 273 K < T < 323 K were provided by Olson [19] (AAD_{LT} = 0.21%). They were also reproduced within 0.3%. Again, ancillary equations by DIPPR [30] and TDE [20] were used to obtain an impression whether the trend of the present FEOS is reasonable. Up to T = 385 K, the DIPPR equation [30] was reproduced within 1%. The TDE [20] calculations follow the FEOS within 1% up to T = 425 K. For both ancillary equations, the deviations are larger in the higher temperature region. This trend could be caused due to fitting the ancillary equations to the data by Walters & Smith [5], which show the systematic offset discussed before.

For the saturated vapor density, only the two datasets by Walters & Smith [5] and Olson [19] were published. Because of large deviations they were not considered in the present fit. The deviation plot, including the ancillary equation of TDE [20], can be found in Fig. 6. A DIPPR correlation is not available.

The speed of sound was investigated by Hurly [8]. Hurly [8] reported a general uncertainty of their apparatus of 0.01%. Regarding the sample preparation, an overall uncertainty of about 0.1% for these data was assumed. Fig. 7 shows that most of the data were represented within 0.15% for T < 360 K. Approaching the phase boundary, the deviations increase up to 0.2%. Data at higher temperatures were reproduced within the claimed uncertainty of 0.1%.

In Fig. 8, comparisons of the FEOS for the heat of vaporization and the isobaric heat capacity of the saturated liquid are illustrated. A few experimental data points are available for the heat of vaporization. Data by Giauque & Gordon [11] and Lide [7] were represented within 0.22%. Other measurements were fitted within 1%. Additionally, several correlations, i.e. TDE [20], DIPPR [30] and Yaws [36], were considered. They show different trends, and further experimental measurements are needed to decide which one is correct. For the isobaric heat capacity of the saturated liquid phase, data by Giauque & Gordon [11] were considered. They were reproduced within 0.7%.

As mentioned above, there are only VLE and gas phase laboratory measurements available. Therefore, molecular simulation data based on the molecular model by Eckl et al. [52] were applied to the FEOS fit. In this way, the homogeneous liquid phase as well as the supercritical region can be described. Fig. 9 shows selected deviations of the residual Helmholtz energy A^{r}_{00} as well as its derivatives A^{r}_{xy} up to the second order. Note that

$$\begin{aligned} A_{xy} = A^{\mathrm{o}}_{xy} + A^{\mathrm{r}}_{xy} &= \tau^x \delta^y \frac{\partial^{x+y} \alpha(\tau,\delta)}{\partial \tau^x \partial \delta^y} \\ &= (1/T)^x \rho^y \frac{\partial^{x+y} \alpha(1/T,\rho)}{\partial (1/T)^x \partial \rho^y}, \end{aligned} \tag{7}$$

for $\tau = T_{\mathrm{c}}/T$ and $\delta = \rho/\rho_{\mathrm{c}}$, because the critical the values of temperature T_{c} and density ρ_{c} are constants. Comprehensive comparisons of all simulation data can be found in the supplementary material. Overall, the deviations are as follows: A^{r}_{00} = 5%, A^{r}_{01} = 6%, A^{r}_{10} = 5%, A^{r}_{02} = 20%, A^{r}_{20} = 15%, and A^{r}_{11} = 5%. For all properties, deviations increase for low densities, where the fluid approaches ideal gas behavior. This is likely caused by two factors: (1) The contribution from the residual Helmholtz energy to the total property A_{xy} becomes smaller with decreasing density. (2) The numerical values of the derivatives A^{r}_{xy} become significantly smaller in absolute terms with decreasing density, thus the error of molecular modeling is more pronounced when deviations with respect to the FEOS are expressed in relative terms. Additionally, isotherms crossing the zero line have to

be taken into account. E.g. at $T = 450$ K, the property A^{r}_{00} changes from negative to positive between $\rho = 10$ mol $\cdot$ dm^{-3} and $\rho = 12$ mol $\cdot$ dm^{-3}. This behavior can also be found for A^{r}_{01} at $T = 500$ K between $\rho = 14$ mol $\cdot$ dm^{-3} and $\rho = 16$ mol $\cdot$ dm^{-3} and at $T = 800$ K between $\rho = 8$ mol $\cdot$ dm^{-3} and $\rho = 10$ mol $\cdot$ dm^{-3}. Despite the fact that the residual Helmholtz energy and its derivatives are not common fluid properties, the A^{r}_{xy} values are related to well known properties like pressure p, speed of sound w, isobaric heat capacity c_p, and isochoric heat capacity c_v

$$\frac{p}{\rho RT} = 1 + A^{r}_{01}, \tag{8}$$

$$\frac{Mw^2}{RT} = 1 + 2A^{r}_{01} + A^{r}_{02} - \frac{(1 + A^{r}_{01} - A^{r}_{11})^2}{A^{o}_{20} + A^{r}_{20}}, \tag{9}$$

$$\frac{c_p}{R} = -(A^{o}_{20} + A^{r}_{20}) + \frac{(1 + A^{r}_{01} - A^{r}_{11})^2}{1 + 2A^{r}_{01} + A^{r}_{02}}, \tag{10}$$

$$\frac{c_v}{R} = -(A^{o}_{20} + A^{r}_{20}), \tag{11}$$

where M is the molar mass. Fig. 10 shows that the overall deviation of 6% in terms of A^{r}_{01} causes deviations of about 4 % in terms of pressure. Because the speed of sound and the heat capacities are caloric properties, the second derivative of the ideal Helmholtz energy with respect to the temperature A^{o}_{20} is needed. It was calculated from Eq. (2). In addition to the ideal part, A^{r}_{01}, A^{r}_{02}, A^{r}_{11}, and A^{r}_{20} are involved. Although deviations between 5% to 20% occur for these properties, deviations in terms of density, isochoric heat capacity, and speed of sound are 2%, 2%, and 4%, respectively. Deviations increase for higher densities.

Special attention has to be given to physically reasonable behavior of the FEOS. Therefore, several thermodynamic properties, e.g. speed of sound, isochoric and isobaric heat capacity, VLE, virial coefficients, and the ideal curves, were studied. Fig. 11 shows a summary of the most important diagrams. The extrapolation behavior of the thermodynamic properties is well-known [54, 55], and all of these plots show physically reasonable properties. In the T versus ρ diagram (Fig. 11, top left) the rectilinear diameter is a straight line up to the critical point and the critical isotherm shows a distinctive sattle point at the critical point. In the p versus ρ diagram (Fig. 11, top right) the isotherms should converge, but not cross each other at high temperatures, pressures, and densities. The speed of sound (Fig. 11, center left) should show a negative slope and no curvature at low temperatures in the hypothetical liquid phase. As expected, the saturated liquid and vapor lines meet as a minimum at the critical point. For the residual isochoric heat capacity (Fig. 11, center right), the saturated liquid line has a positive curvature and rises towards low temperatures. Related to the minimum at the critical point of the speed of sound, a maximum for the residual isochoric heat capacity can be observed. The second and third thermal virial coefficients B and C should be negative for low temperatures, cross the zero line once, and then approach zero after passing through a maximum. For B, the maximum occurs at the Boyle temperature, and for C, the maximum occurs at the critical point. The ideal curves should be smooth and show no unusual curvature. Except for small irregularities in the Joule and Joule-inversion curves, the ideal curves (Fig. 11, bottom right) show a reasonable behavior.

Conclusion

A fundamental equation of state for ethylene oxide was presented. It is given in terms of the Helmholtz energy and can be used to calculate all thermodynamic properties, including density, heat capacities, speed of sound, enthalpy, internal energy, and vapor-liquid equilibria. It is based on a hybrid dataset so that two different classifications for the range of validity have to be made. The experimental data cover temperatures from the triple point up to the critical point. Ethylene oxide was experimentally investigated only little so that the range of validity covered by experimental data includes the homogeneous vapor phase and the vapor-liquid equilibrium. Based on these investigations and a careful analysis of the extrapolation behavior, the range of validity based on experimental data is over a temperature range from the triple point T_{tr} to 500 K, with a maximum pressure of p_{max}

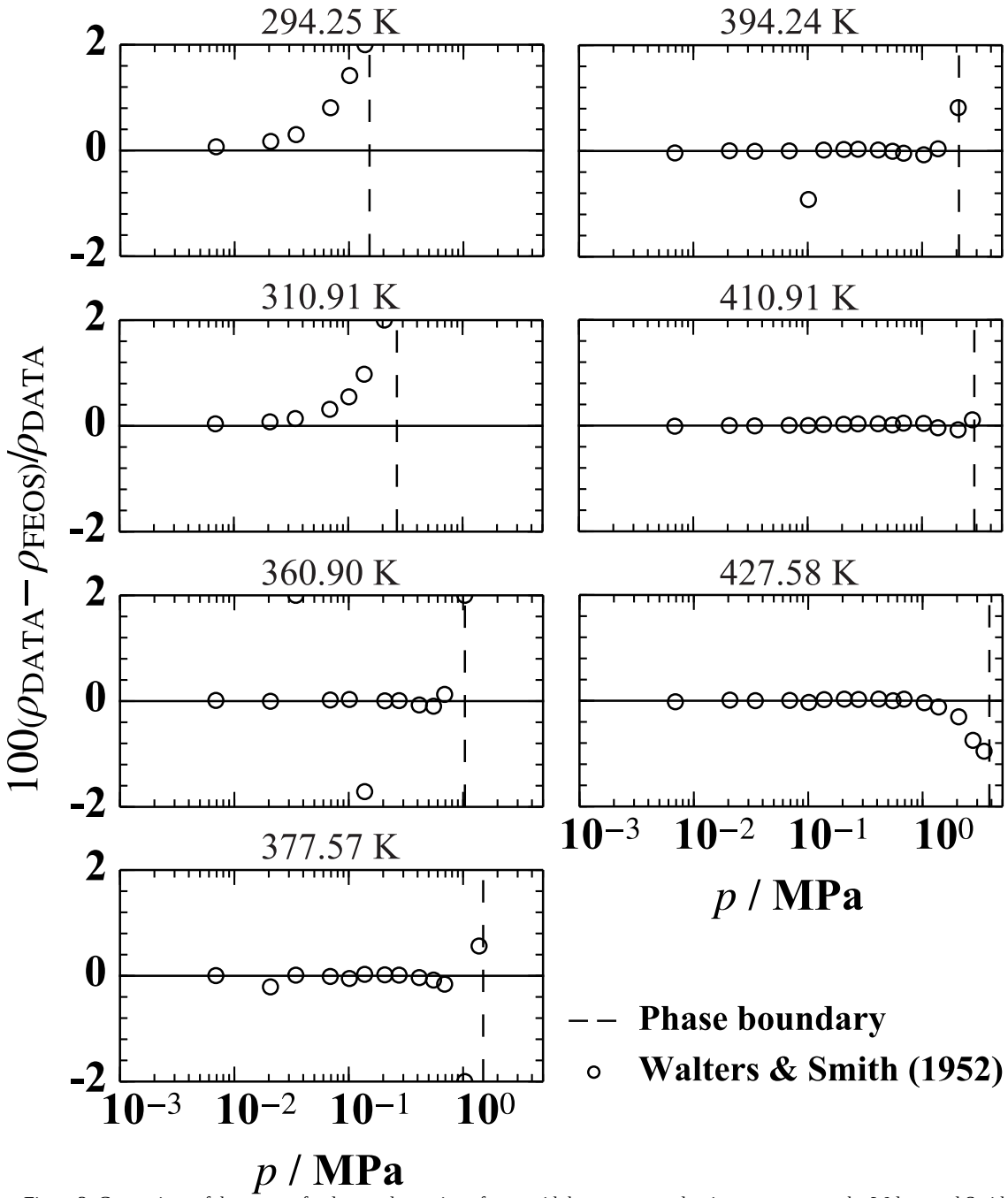

Figure 3: Comparison of the present fundamental equation of state with homogeneous density measurements by Walters and Smith [5].

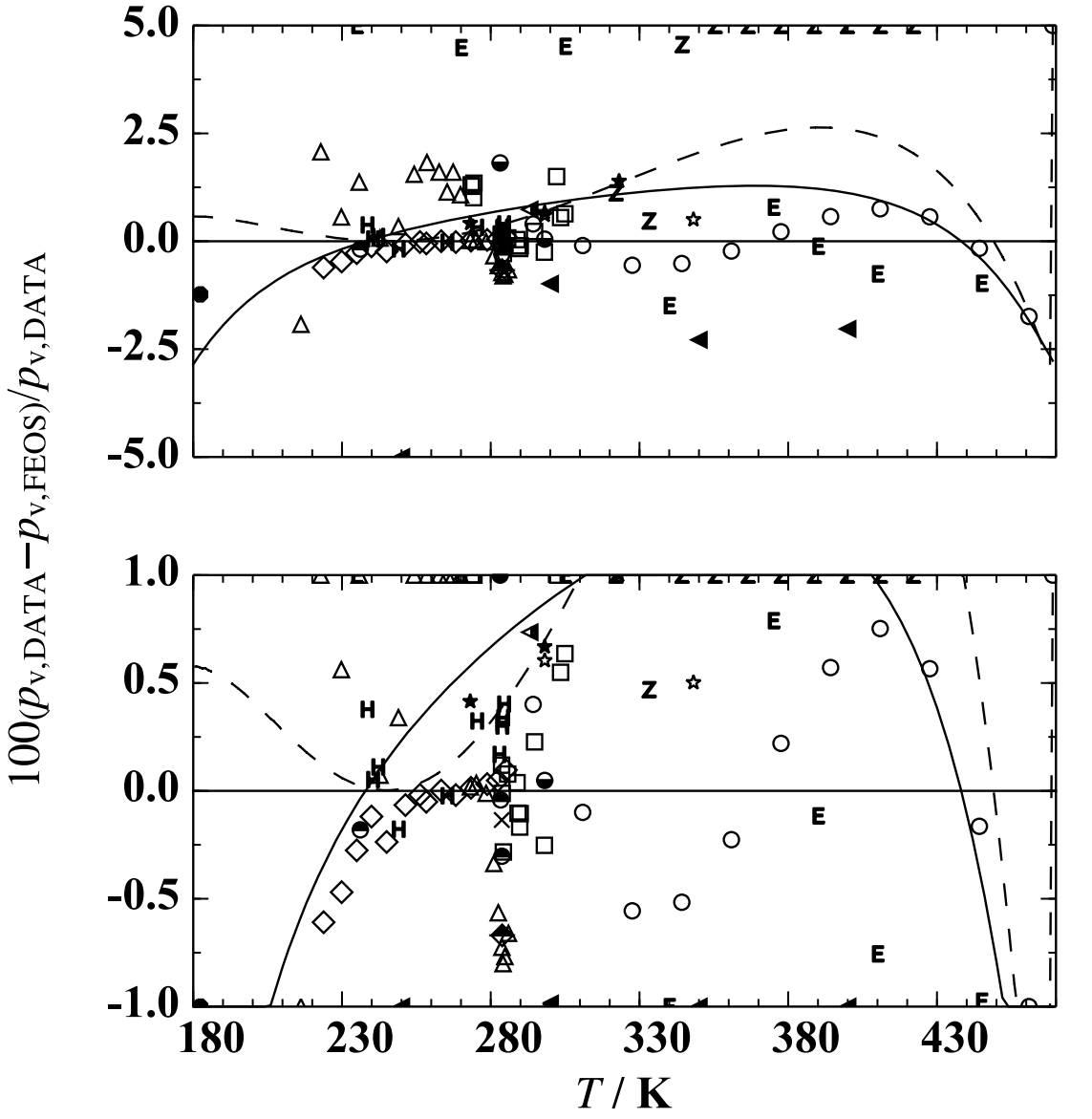

- Calado *et al*. (1996)
- Chao *et al*. (1986)
- Coles & Popper (1950)
- DIPPR (2006)*
- Eckl *et al*. (2008)§
- Giauque & Gordon (1949)
- Giles & Wilson (2006)
- Gillespie *et al*. (1985)
- Hess & Tilton (1950)
- Kistiakowsky & Rice (1940)
- Lide (2005)
- Maass & Boomer (1922)
- McDonald *et al*. (1959)
- Mock & Smith (1950)
- Olson (1977)
- TDE (2013)*
- This work§
- Walters & Smith (1952)

Figure 4: Comparison of the present fundamental equation of state with vapor pressure data. The asterisk marks ancillary equations and the paragraph symbol stands for molecular simulation data.

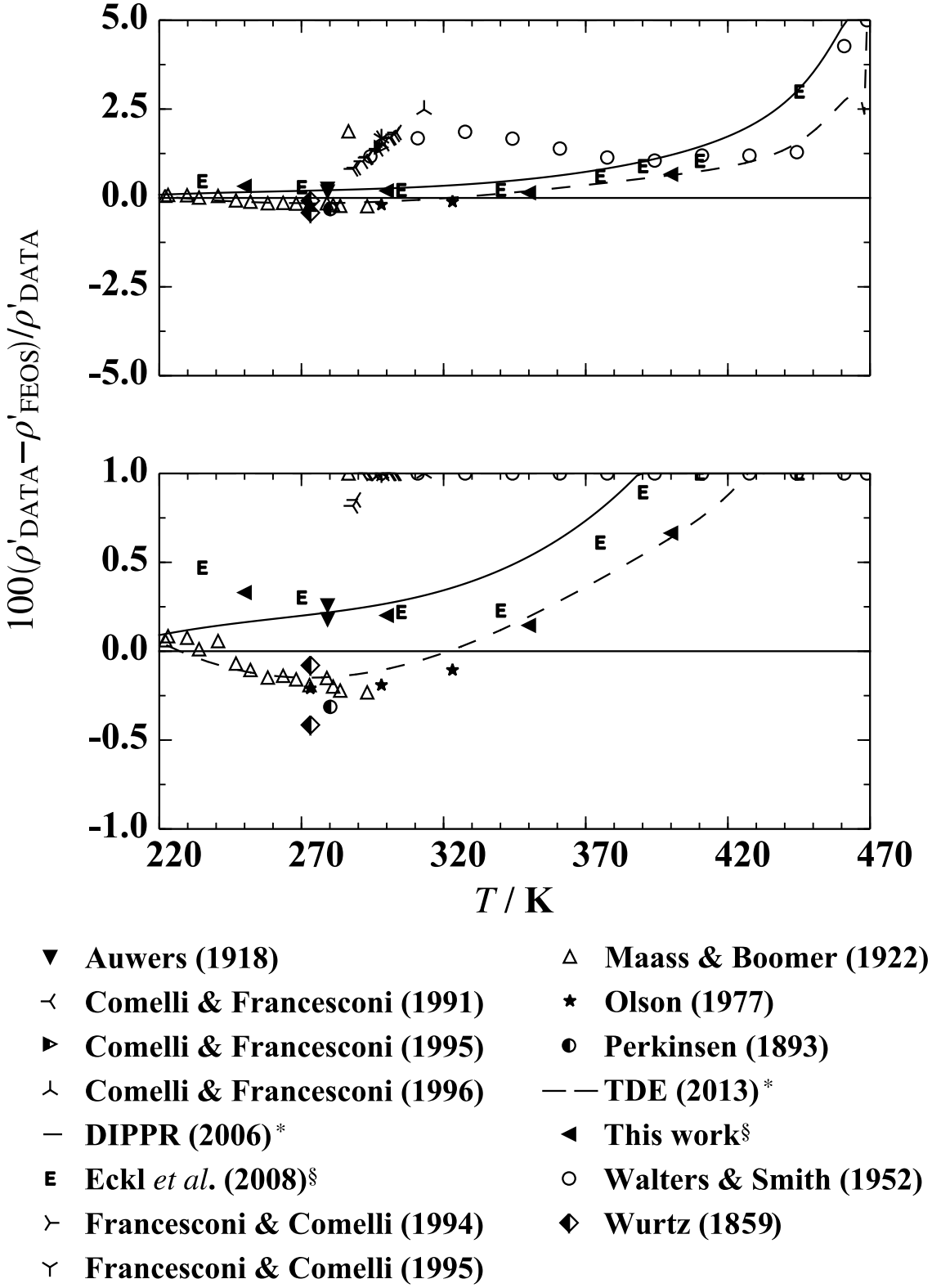

Figure 5: Comparison of the present fundamental equation of state with saturated liquid density data. The asterisk marks ancillary equations and the paragraph symbol stands for molecular simulation data.

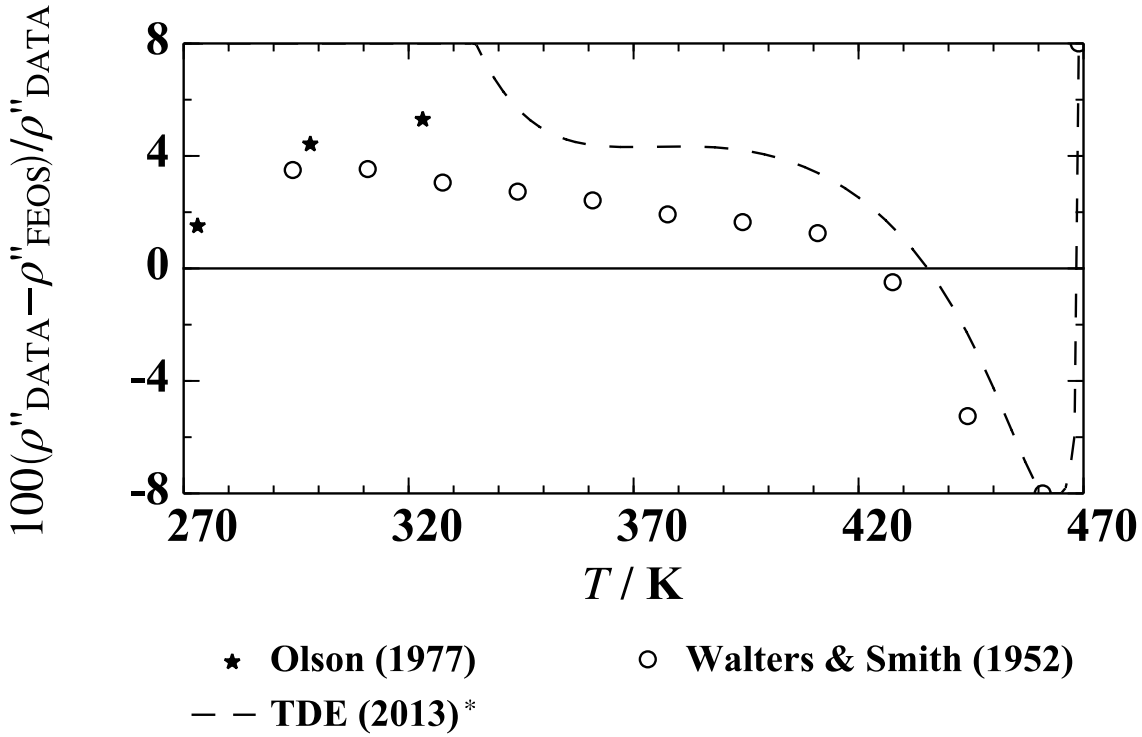

Figure 6: Comparison of the present fundamental equation of state with saturated vapor density data. The asterisk marks ancillary equations.

Table 3: Average absolute relative deviations between experimental or simulation results and the values calculated from the present fundamental equation of state.

Source	AAD/%					
	Vap.	Liq.	Crit.	LD	MD	HD
Simulation data (this work)						
A^r_{00}	5.78	0.79	1.30	3.68	9.45	4.01
A^r_{01}	7.37	14.0	1.05	2.61	2.26	9.33
A^r_{02}	78.6	9.54	4.74	17.4	4.19	10.3
A^r_{10}	4.11	0.67	4.06	5.27	1.78	0.82
A^r_{11}	5.30	6.10	2.33	3.36	1.38	3.02
A^r_{20}	10.7	5.33	13.6	6.54	8.31	6.91
Homogeneous density						
Walters & Smith (1952) [5]	0.28					
Speed of sound						
Hurly (2002) [8]	0.05					
Isobaric heat capacity						
Giauque & Gordon (1949) [11]		0.22				
Enthalpy of vaporization						
Giauque & Gordon (1949) [11]	0.02					
Lange & Dean (1973) [31]	0.11					
Lide (2005) [7]	0.13					
Washburn (1933) [35]	0.54					
Cox & Pilcher (1970) [29]	0.53					
Reid et al. (1977) [33]	0.29					
Timmermans (1965) [34]	0.84					
Eckl et al. (2008) [52]	2.05					
this work	1.01					
Ideal isobaric heat capacity						
Chao et al. (1986) [6]	0.54					
Dorofeeva (1992) [37]	0.49					
Guenthard & Heilbronner (1948) [41]	0.65					
Guenthard et al. (1950) [40]	0.37					
Hurly (2002) [8]	0.40					
Kistiakowsky & Rice (1940) [15]	0.18					
Lange & Dean (1973) [31]	0.12					
Ramasamy & Srinivasacharya (1978) [42]	1.25					
Walters & Smith (1952) [5]	0.36					
Sundaram (1963) [43]	0.04					
Godnev & Morozov (1948) [39]	0.27					
Vvedenskii (1969) [44]	0.10					

(Vap.) homogeneous vapor phase
(Liq.) homogeneous liquid phase
(Crit.) $0.98T_c < T < 1.1T_c$ and $0.7\rho_c < \rho < 1.4\rho_c$
(LD) $\rho < 0.6\rho_c$ and $T > T_c$
(MD) $0.6\rho_c \le \rho \le 1.5\rho_c$ and $T > T_c$
(HD) $\rho > 1.5\rho_c$ and $T > T_c$

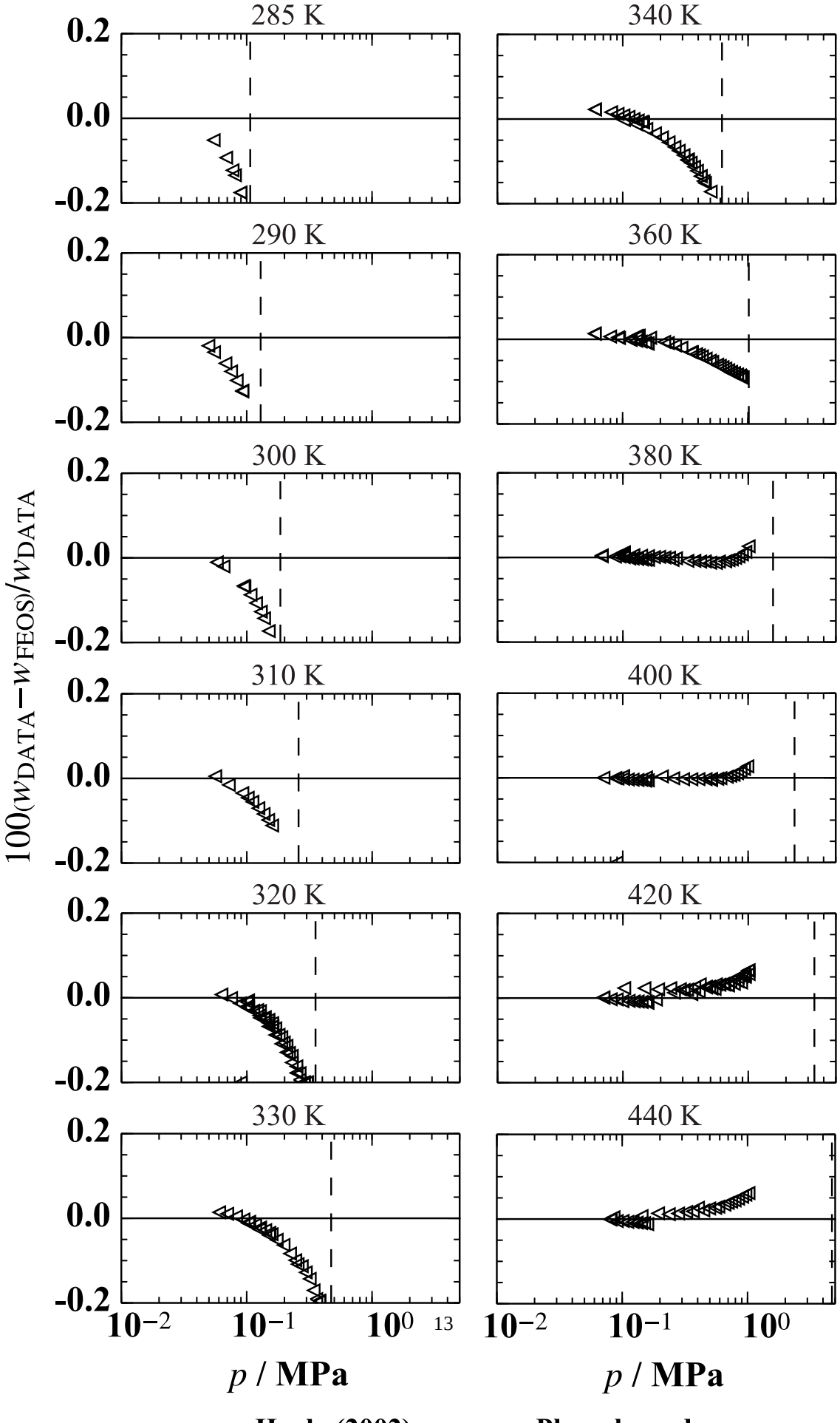

Figure 7: Comparison of the present fundamental equation of state with experimental speed of sound data by Hurly [8].

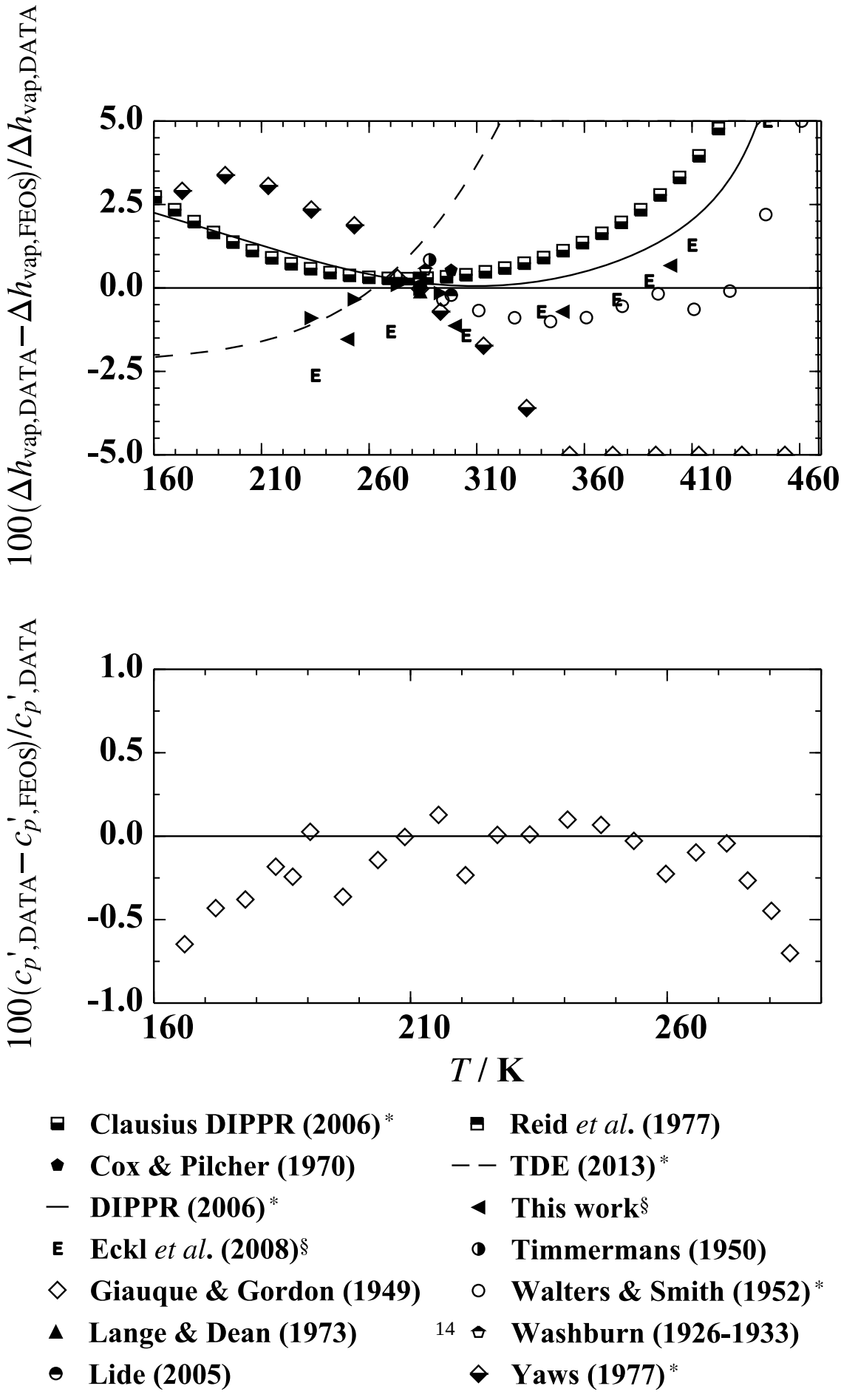

Figure 8: Comparisons of the present fundamental equation of state for the enthalpy of vaporization (top) and the isobaric heat capacity of the saturated liquid phase (bottom). The asterisk marks ancillary equations and the paragraph symbol denotes molecular simulation data.

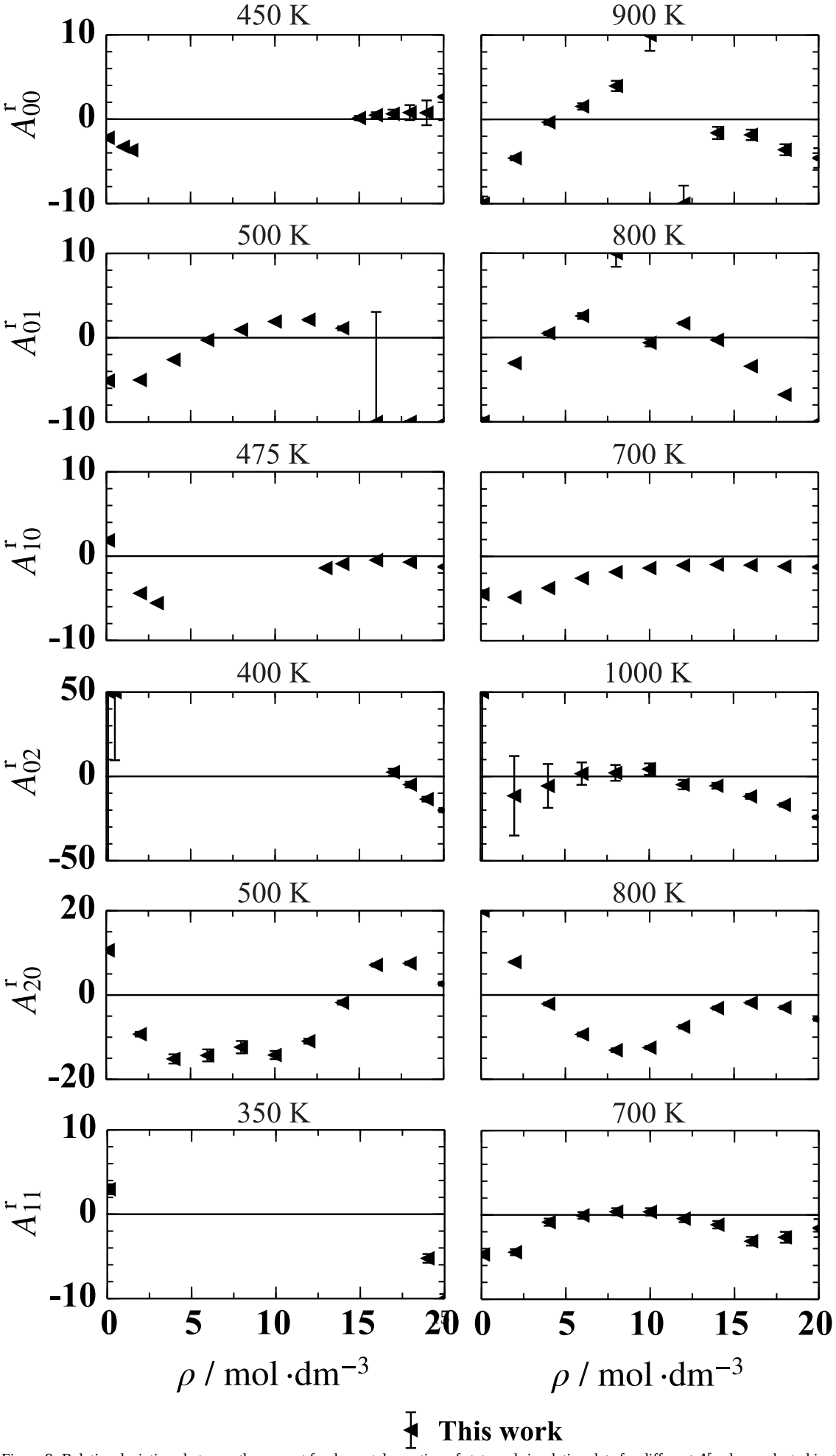

Figure 9: Relative deviations between the present fundamental equation of state and simulation data for different A^r_{xy} along selected isotherms.

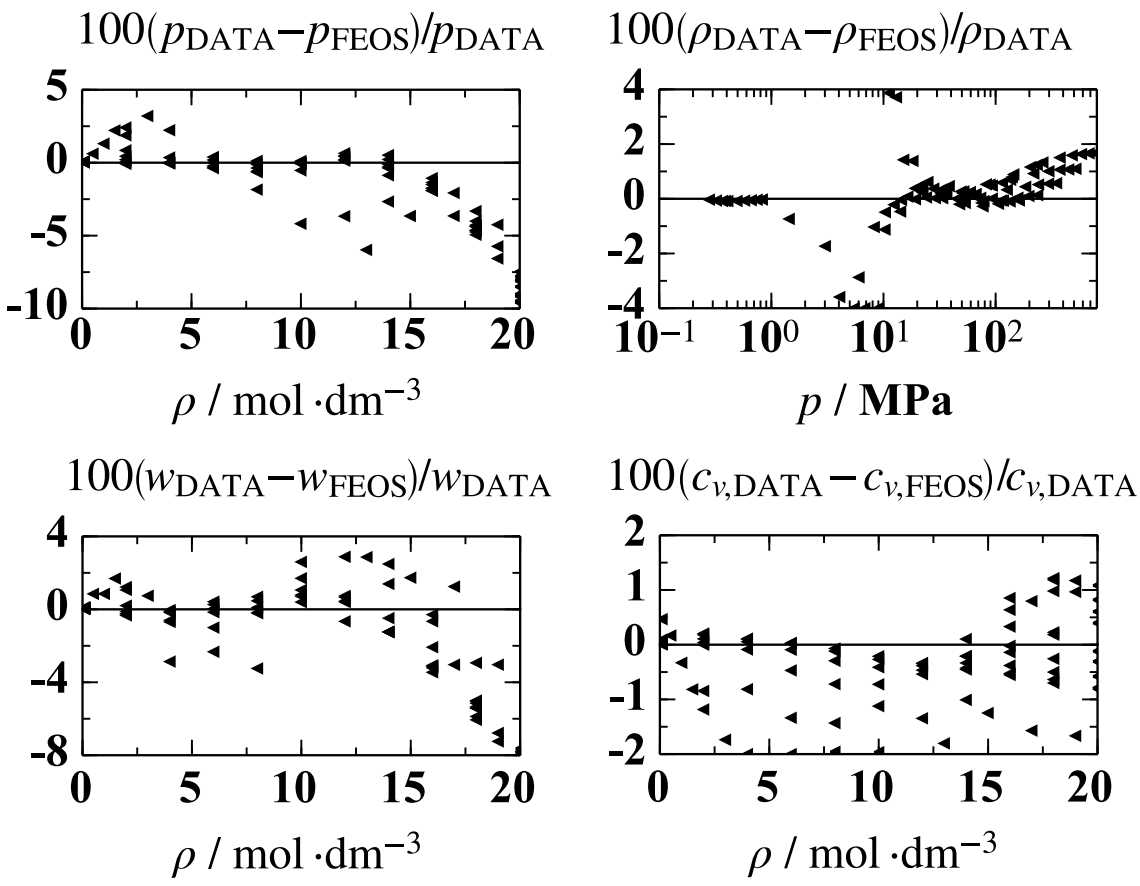

Figure 10: Comparison of the present fundamental equation of state with thermodynamic properties obtained from molecular simulation data.

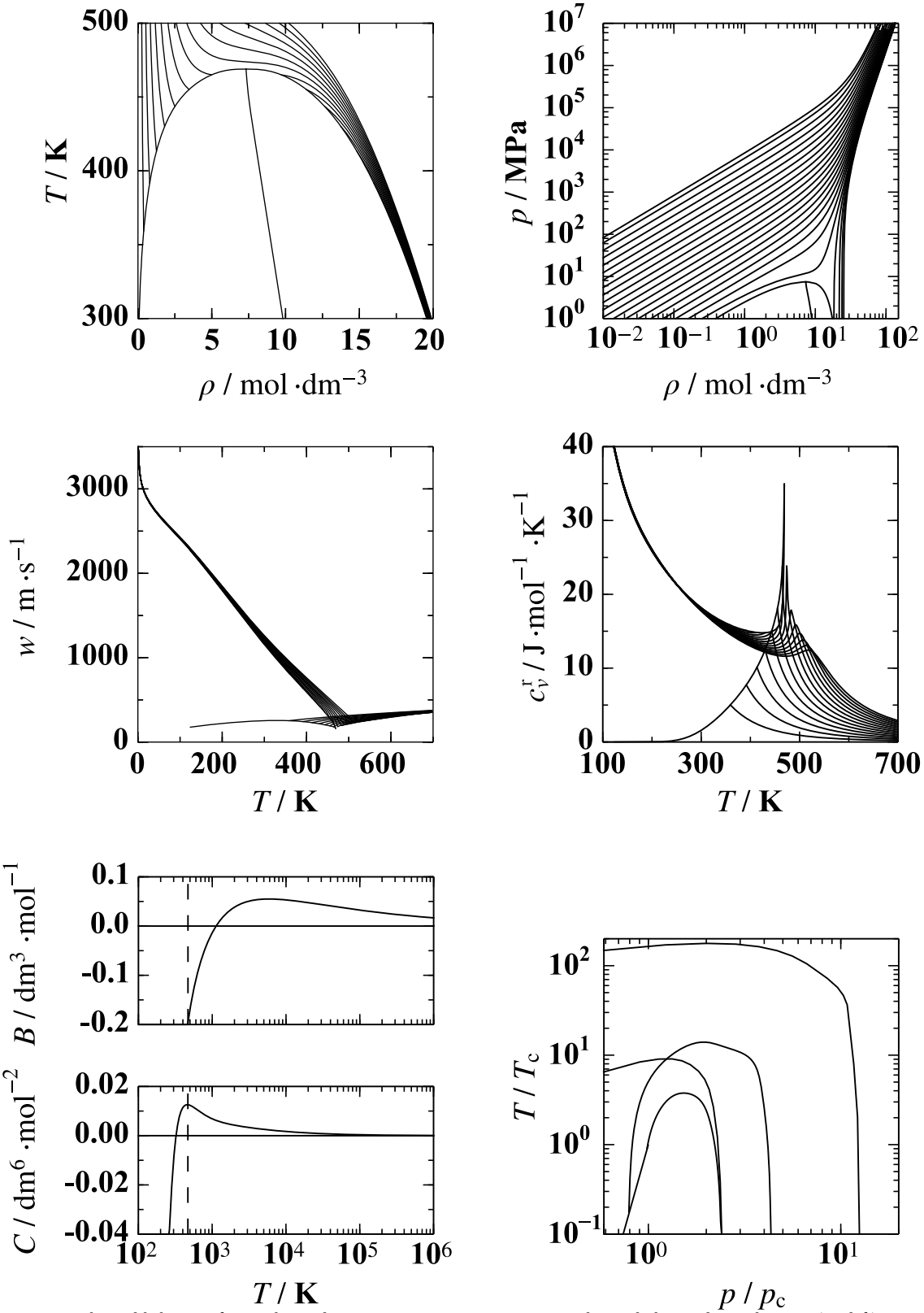

Figure 11: Physical behavior of some thermodynamic properties: VLE curves together with the rectilinear diameter (top left), $p\rho T$ data at extreme conditions (top right), speed of sound (center left), residual isochoric heat capacity (center right), second and third virial coefficients (bottom left), and ideal curves (bottom right).

Table 4: Average absolute relative deviations between experimental or simulated VLE data and the values calculated from the present fundamental equation of state.

Source	AAD/%		
	LT	MT	HT
Vapor pressure			
Olson (1977) [19]	0.41	1.03	
Calado et al. (1996) [9]	1.23		
Chao et al. (1986) [6]		0.13	
Coles & Popper (1950) [10]	1.23	0.31	
Giauque & Gordon (1949) [11]	0.16	0.07	
Giles & Wilson (2006) [12]		0.55	
Hess & Tilton (1950) [14]		0.74	
Kistiakowsky & Rice (1940) [15]		0.67	
Lide (2005) [7]	0.18	0.17	
Maass & Boomer (1922) [16]	0.97	0.70	
McDonald et al. (1959) [17]	0.18	0.31	
Walters & Smith (1952) [5]		0.41	1.74
Mock & Smith (1950) [18]		7.52	
Gillespie et al. (1985) [13]		0.93	
This work	22.80	1.77	
Saturated liquid density			
Olson (1977) [19]	0.21	0.15	
Wurtz (1859) [28]	0.25		
Walters & Smith (1952) [5]		1.36	4.27
Perkinsen (1893) [27]	0.31		
Maass & Boomer (1922) [16]	0.11	0.78	
Francesconi & Comelli (1995) [26]		1.67	
Francesconi & Comelli (1994) [25]		1.68	
Comelli & Francesconi (1995) [23]		1.47	
Comelli & Francesconi (1996) [24]		2.08	
Comelli & Francesconi (1991) [22]		1.36	
Auwers (1918) [21]	0.22		
This work	0.33	0.34	
Saturated vapor density			
Walters & Smith (1952) [5]		2.58	19.13
Olson (1977) [19]	1.51	4.86	

(LT) $T < 0.6T_c$
(MT) $0.6T_c \leq T \leq 0.98T_c$
(HT) $T > 0.98T_c$

Table 5: Calculated values of properties for algorithm verification.

T / K	p / MPa	ρ / mol · dm^{-3}	h / J · mol^{-1}	s / J · mol^{-1} · K^{-1}	c_v / J · mol^{-1} · K^{-1}	c_p / J · mol^{-1} · K^{-1}	w / m · s^{-1}	a / J · mol^{-1}
200 [a]	0.0007171788	22.4762797391	-33442.98983	-122.0751209	54.1084845521	81.5266043374	1794.54046849	-9027.99755819
200 [b]	0.0007171788	0.0004315688	-4103.02312658	24.6247126168	28.276210133	36.6153026833	220.943064557	-10689.7605167
300 [a]	0.1852431635	19.5606827885	-25005.6597986	-88.0098778297	58.0568818562	89.6975069336	1152.98334772	1387.83337153
300 [b]	0.1852431635	0.0776886235	-298.78451672	-5.6536268902	41.4426537002	51.8388241926	254.127483231	-987.127466278
400 [a]	2.3448898851	15.5640200379	-14928.2462422	-59.5392920537	69.0464048677	117.352380776	590.414507618	8736.80963958
400 [b]	2.3448898851	0.9448808588	2699.82561728	-15.4691124051	62.6390709898	93.32073484	238.903280942	6405.79274309
500	1	0.2509683066	11943.4908179	11.6066851136	67.9588531662	78.0665039031	315.413932985	2155.58138999
500	10	5.5466493279	2602.95313485	-22.6269845215	81.9472541876	256.331691752	214.249497553	12113.5551444

(a) saturated liquid phase
(b) saturated vapor phase

= 10 MPa. The uncertainties of the homogeneous density in the gaseous phase are 0.1% for $T > 360$ K and up to 0.6% for lower temperatures. The uncertainties of the vapor pressure are 0.5% for T <300 K and up to 0.8% for higher temperatures. For the saturated liquid density, it is difficult to make a statement on the uncertainty because of the poor data situation. It is about 0.25% for $T < 300$ K, and up to 1.5% for higher temperatures. The speed of sound in the gaseous phase was reproduced within 0.15% for $T < 360$ K. Higher temperatures were represented within 0.1%. All deviations are larger in the critical region. Using molecular simulation data, the range of validity was extended to the liquid state up to a maximum temperature and pressure of $T_{\max} = 1000$ K and $p_{\max} = 700$ MPa. Because of the special data situation, the physical behavior of the FEOS in regions where no experimental data are available was carefully monitored. The extrapolation behavior is reasonable. Reference values are given in Table 5 to verify computer implementation of the FEOS.

Acknowledgments

The authors gratefully acknowledge financial support by Deutsche Forschungsgemeinschaft under the grants VR6/4-1 and SP507/7-1.The programming effort was funded by BMBF under the project ”01IH13005A SkaSim: Skalierbare HPC-Software fr molekulare Simulationen in der chemischen Industrie”. This work was carried out under the auspices of the Boltzmann-Zuse Society (BZS) of Computational Molecular Engineering. The simulations were carried out on the Cray XE6 (Hermit) at the High Performance Computing Center Stuttgart (HLRS).

Appendix A. Ancillary equations

For computer calculations it is helpful to use ancillary equations to generate starting values for density iterations. Therefore ancillary equations for vapor pressure, saturated liquid density, and saturated vapor density were developed. The equations and parameters are given below, cf. Table A.6. These ancillary equations are not reference equations, thus the FEOS has to be used in order to calculate accurate saturation properties.
Vapor pressure:

$$\ln \frac{p_v}{p_c} = \frac{T_c}{T} \sum_{i=1}^{5} n_i \left(1 - \frac{T}{T_c}\right)^{t_i} . \tag{A.1}$$

Saturated liquid density:

$$\ln \frac{\rho'}{\rho_c} = \sum_{i=1}^{5} n_i \left(1 - \frac{T}{T_c}\right)^{t_i} . \tag{A.2}$$

Saturated vapor density:

$$\ln \frac{\rho''}{\rho_c} = \sum_{i=1}^{6} n_i \left(1 - \frac{T}{T_c}\right)^{t_i} . \tag{A.3}$$

Table A.6: Parameter values of the present ancillary equations for vapor pressure, saturated liquid density, and saturated vapor density.

	Eq. (A.1)		Eq. (A.2)		Eq. (A.3)	
i	n_i	t_i	n_i	t_i	n_i	t_i
1	-0.74136D+01	1	0.6610D+00	0.25	-0.10592D+01	0.3
2	0.19870D+01	1.5	0.4045D+01	0.7	-0.10712D+02	0.91
3	-0.66330D+01	3.5	-0.4488D+01	1.2	0.16812D+02	1.6
4	0.71500D+01	4.3	0.3445D+01	1.75	-0.27664D+02	2.26
5	-0.47200D+01	5.2	-0.9230D+00	2.4	-0.54968D+02	6.6
6					-0.20428D+03	17

Table B.7: Sigma (σ) and epsilon (ϵ) denote the length and energy parameter of the Lennard-Jones (LJ) potential, respectively. k_B is the Boltzmann constant. μ denotes the dipole moment of the point dipole. All coordinates are in principal axes with respect to the center of mass. The orientation of the point dipole is defined with Euler angles: φ is the azimuthal angle with respect to the x-y-plane and θ is the inclination angle with respect to the z-axis.

Site	x/Å	y/Å	z/Å	σ/Å	$\frac{\epsilon}{k_B}$/K	θ/deg	φ/deg	μ/D
CH_2	0.78	0	-0.48431	3.5266	84.739			
CH_2	-0.78	0	-0.48431	3.5266	84.739			
O	0	0	0.73569	3.0929	62.126			
Dipole	0	0	0			0	0	2.459

Appendix B. Molecular model

The coordinates and parameters for the molecular model of ethylene oxide are given in Table B.7.

[1] R. Span, Multiparameter Equations of State: An Accurate Source of Thermodynamic Property Data, Springer Verlag, Berlin, 2000.
[2] Industrial fluid properties simulation collective, http://fluidproperties.org/.
[3] G. Rutkai, M. Thol, R. Lustig, R. Span, J. Vrabec, The Journal of Chemical Physics 139 (2013) 041102.
[4] P. J. Mohr, B. N. Taylor, D. B. Newell, Reviews of Modern Physics 84 (2012) 1527–1605.
[5] C. J. Walters, J. M. Smith, Chemical Engineering Progress 48 (1952) 337.
[6] J. Chao, K. R. Hall, K. N. Marsh, R. C. Wilhoit, Journal of Physical and Chemical Reference Data 15 (1986) 1369.
[7] D. R. Lide, CRC Handbook of Chemistry and Physics, 86 ed., Taylor and Francis, London, 2005.
[8] J. J. Hurly, International Journal of Thermophysics 23 (2002) 667–696.
[9] J. C. G. Calado, U. K. Deiters, E. J. M. Filipe, The Journal of Chemical Thermodynamics 28 (1996) 201–207.
[10] K. F. Coles, F. Popper, Industrial and Engineering Chemistry 42 (1950) 1434–1438.
[11] W. F. Giauque, J. Gordon, Journal of the American Chemical Society 71 (1949) 2176–2181.
[12] N. F. Giles, G. M. Wilson, Journal of Chemical and Engineering Data 51 (2006) 1954–1962.
[13] P. C. Gillespie, J. R. Cunningham, G. M. Wilson, AIChE symposium series 81 (1985) 26–40.
[14] L. G. Hess, V. V. Tilton, Industrial and Engineering Chemistry 42 (1950) 1251–1258.
[15] G. B. Kistiakowsky, W. W. Rice, The Journal of Chemical Physics 8 (1940) 618–622.
[16] O. Maass, E. H. Boomer, Journal of the American Chemical Society 44 (1922) 1709–1728.
[17] R. A. McDonald, S. A. Shrader, D. R. Stull, Journal of Chemical and Engineering Data 4 (1959) 311–313.
[18] J. E. Mock, J. M. Smith, Industrial and Engineering Chemistry 42 (1950) 2125–2128.
[19] J. D. Olson, Journal of Chemical and Engineering Data 22 (1977) 326–329.
[20] M. Frenkel, R. D. Chirico, V. Diky, K. Kroenlein, C. D. Muzny, A. F. Kazakov, J. W. Magge, I. M. Abdulagatov, E. W. Lemmon, NIST Standard Reference Database 103b: NIST Thermo–Data Engine – Pure Compounds, Binary Mixtures, Reactions, Version 8.0: National Institute of Standards and Technology, Standard Reference Data Program, Gaithersburg.
[21] K. V. Auwers, Justus Liebig's Annalen der Chemie 415 (1918) 98–168.
[22] F. Comelli, R. Francesconi, Journal of Chemical and Engineering Data 36 (1991) 382–383.
[23] F. Comelli, R. Francesconi, Journal of Chemical and Engineering Data 40 (1995) 28–30.
[24] F. Comelli, R. Francesconi, Journal of Chemical and Engineering Data 41 (1996) 101–104.
[25] R. Francesconi, F. Comelli, Journal of Chemical and Engineering Data 39 (1994) 106–107.
[26] R. Francesconi, F. Comelli, Journal of Chemical and Engineering Data 40 (1995) 512–514.
[27] W. H. Perkin, Journal of the Chemical Society, Transactions 63 (1893) 488–491.
[28] A. Wurtz, Annales de chimie et de physique 55 (1859) 433.
[29] J. D. Cox, G. Pilcher, Thermochemistry of Organic and Organometallic Compounds, Academic Press, New York, 1970.
[30] R. L. Rowley, W. V. Wilding, J. L. Oscarson, Y. Yang, , N. A. Zundel, T. E. Daubert, R. P. Danner, DIPPR Data Compilation of Pure Compound Properties: Design Institute for Physical Properties, AIChE, New York, 2006.
[31] N. A. Lange, J. A. Dean, Lange's Handbook of Chemistry, 11 ed., McGraw–Hill, New York, 1973.
[32] M. Company, Matheson Gas Data Book, 6 ed., Lyndhurst, New Jersey, 1980.
[33] R. C. Reid, J. M. Prausnitz, T. K. Sherwood, The Properties of Gases and Liquids, 3 ed., McGraw–Hill, New York, 1977.
[34] J. Timmermans, Physico–Chemical Constants of Pure Organic Substances: Vol II, New York, New York, 1965.
[35] E. W. Washburn, International Critical Tables of Numerical Data, Physics, Chemistry, and Technology: 7 Vols + Index, McGraw–Hill, New York, 1926–1933.
[36] C. L. Yaws, Physical Properties: A Guide to the Physical, Thermodynamic, and Transport Property Data of Industrially Important Chemical Compounds, McGraw–Hill, New York, 1977.
[37] O. V. Dorofeeva, Thermochimica Acta 194 (1992) 9–46.
[38] M. Frenkel, G. J. Kabo, K. N. Marsh, G. N. Roganov, R. C. Wilhoit, Thermodynamics of Organic Compounds in the Gas State (Volumes I and II), Thermodynamics Research Center, College Station, TX, 1994.
[39] I. Godnev, V. Morozov, Zhurnal Fizicheskoi Khimii 22 (1948) 801–803.

[40] H. H. Guenthard, B. Messikommer, M. Kohler, Helvetica Chimica Acta 33 (1950) 1809–1823.
[41] H. Guenthard, E. Heilbronner, Helvetica Chimica Acta 31 (1948) 2128–2132.
[42] R. Ramasamy, K. G. Srinivasacharya, Current Science 47 (1978) 668–669.
[43] S. Sundaram, Zeitschrift fuer Physikalische Chemie (Muenchen) 36 (1963) 376–377.
[44] A. A. Vvedenskii, Zurnal Fiziceskoj Chimii 40 (1969) 1953–1955.
[45] R. Lustig, Molecular Simulation 37 (2011) 457–465.
[46] R. Lustig, Molecular Physics 110 (2012) 3041–3052.
[47] S. Deublein, B. Eckl, J. Stoll, S. V. Lishchuk, G. Guevara-Carrion, C. W. Glass, T. Merker, M. Bernreuther, H. Hasse, J. Vrabec, Computer Physics Communications 182 (2011) 2350–2367.
[48] C. W. Glass, S. Reiser, G. Rutkai, S. Deublein, A. Köster, G. Guevara-Carrion, A. Wafai, M. Horsch, M. Bernreuther, T. Windmann, H. Hasse, J. Vrabec, Computer Physics Communications, (in press), http://dx.doi.org/10.1016/j.cpc.2014.07.012
[49] D. Frenkel, B. Smit, Understanding Molecular Simulation: From Algorithms to Applications, Academic Press, Elsevier, San Diego, 2002.
[50] J. A. Barker, R. O. Watts, Mol. Phys. 26 (1973) 789–792.
[51] B. Widom, The Journal of Chemical Physics 39 (1963) 2808–2812.
[52] B. Eckl, J. Vrabec, H. Hasse, Fluid Phase Equilibria 274 (2008) 16–26.
[53] F. H. Case, J. Brennan, A. Chaka, K. D. Dobbs, D. G. Friend, P. A. Gordon, J. D. Moore, R. D. Mountain, J. D. Olson, R. B. Ross, M. Schiller, V. K. Shen, E. A. Stahlberg, Fluid Phase Equilibria 274 (2008) 2–9.
[54] E. W. Lemmon, R. T. Jacobsen, Journal of Physical and Chemical Reference Data 34 (2005) 69–108.
[55] E. W. Lemmon, M. O. McLinden, W. Wagner, Journal of Chemical and Engineering Data 54 (2009) 3141–3180.